J. Fluid Mech. (1991), *vol.* 232, *pp.* 611–627
Printed in Great Britain

The onset and development of circular-cylinder vortex wakes in uniformly accelerating flows

By TIM LEE† AND RALPH BUDWIG
Mechanical Engineering Department, University of Idaho, Moscow, ID 83843, USA

(Received 17 October 1990 and in revised form 3 May 1991)

The influence of uniform flow acceleration on the stability and the characteristics of circular-cylinder wakes over a Reynolds-number range, $20 < R < 330$, was investigated. Experiments were performed to examine the temporal evolution of the wake before, during, and after the onset of the wake instability. We have demonstrated in several ways that the wake is stabilized by flow acceleration: (i) the onset of the wake instability occurs at larger Reynolds numbers than in the steady flow case, (ii) the closed wake develops to states that would be unstable in a steady flow, and (iii) once vortex shedding does occur there is a reduction in instantaneous Strouhal number. We have also examined the temporal growth rate of the wake instability and find that it is directly proportional to the applied flow acceleration. Physical mechanisms are proposed to describe the experimental observations.

1. Introduction

The separation of vortices from bluff bodies leading to a vortex street is a well-known phenomenon encountered in many applications. The wake behind a circular cylinder is one such flow; it is of fundamental interest and has been the subject of many experimental, theoretical and numerical studies.

For steady flow above a Reynolds number of 5, and up to the critical value of the Reynolds number, the wake consists of a recirculating zone of two attached symmetric vortices. Both the strength and the length of these vortices increase with increasing Reynolds number (Nishioka & Sato 1974, 1978; Coutanceau & Bouard 1977*a*; and others). As the critical Reynolds number is approached, a ratio of the vortex length to cylinder diameter, S_e/D (S_e is the closed vortex length as measured from the rear of the cylinder to the rear wake stagnation point and D is the cylinder diameter), of about 2.2 is attained. At the critical Reynolds number, R_c, there is a transition characterized by global temporal instability of the wake eventually leading to alternate shedding of the vortices and the formation of a vortex street (see e.g. Monkewitz 1988; Karniadakis & Triantafyllou 1989).

When the flow over the cylinder is accelerating or when the cylinder is accelerated through quiescent fluid the wake can have new features that are not quasi-steady. The instantaneous state as well as the past history of the flow play significant roles in the development of the wake. Most past investigations of unsteady bluff-body flows have concentrated on the initial phase of the development (i.e. the growth of the attached vortices with time). Investigations of the early stages of development include impulsively started flows as well as flows with uniform acceleration. For

† Current address: Chemical Engineering Department, Johns Hopkins University, Baltimore, MD 21218, USA.

impulsively started flows, the time development of the closed wake geometry (with $R < 40$), the motion of separation points, and of the drag coefficients have been investigated by Sarpkaya (1963, 1978), Coutanceau & Bouard (1977*b*), Bouard & Coutanceau (1980). Honji & Taneda (1969), and Taneda (1977) have used flow visualization to examine the early stages of wake geometry development during uniform acceleration with L/D ratios ranging between 4 and 20.

Recently, unsteady flow experiments have been performed at and around the critical Reynolds number in order to reveal the nature of the wake instability. Provansal, Mathis & Boyer (1987) have investigated the disturbance growth rate of cylinders with small cylinder aspect ratios, L/D, by changing wind tunnel speed from subcritical to supercritical. They measured the time development of transverse velocity fluctuations using LDV with the measuring volume at $X/D = 5$ (X is the downstream distance measured from the centre of the cylinder). Sreenivasan, Strykowski & Olinger (1987) measured supercritical growth rates and found that they were independent of measurement position over the range, $5 < X/D < 25$. They concluded that supercritical wake behaviour is well described as a global temporal instability. Both Provansal *et al.* and Sreenivasan *et al.* have found good agreement of disturbance growth rates with the values predicted by the Landau–Stuart equation.

Other than these experiments, data on the time development of the vortex wake at and above the critical Reynolds number are scarce. The influences of unsteadiness on vortex street formation and on the time development of the vortex street are not well understood. The present investigation focuses on the influence of flow acceleration on the temporal evolution of cylinder wakes before, during, and after the onset of wake instability. The following wake characteristics are investigated: (i) the time development of the symmetric attached vortices (closed vortex wake) before transition, (ii) the onset and growth of the wake instability, (iii) the instantaneous shedding frequency of a vortex street, (vi) the combined stabilizing effects along with the end plates. Finally, physical models are proposed to explain the experimental findings.

2. Experimental methods

The wake of a circular cylinder was investigated in a $30 \times 30 \times 183$ cm suction-type unsteady wind tunnel with 25/1 contraction ratio. Two damping tanks ($120 \times 240 \times 120$ cm and $120 \times 240 \times 90$ cm) lined with acoustic tiles were installed between the test section and the fan to prevent fan noise from reaching the test section. The wind speed could be varied from 10 cm/s to 5 m/s and the background turbulence intensity $u'_{\rm rms}/U_0$ was 0.35 % for this velocity range. The test section core velocity profile was uniform to within 0.5 % over the full range of wind speeds. A special fan motor controller was built to allow the generation of repetitive constant accelerating–decelerating wind speed patterns. The input to the controller was a low-level signal from a programmable waveform synthesizer card. The card was programmed to produce voltage waveforms with third-order polynomial ascending and descending profiles. The repetitive sequence of this waveform was in four parts; (i) steady flow with $R_{\rm s} < R_{\rm c}$, (ii) a uniform acceleration ramp, (iii) steady flow with $R_{\rm f} > R_{\rm c}$, and (vi) a uniform deceleration ramp back to $R_{\rm s}$. $R_{\rm s}$ and $R_{\rm f}$ are the initial and final flow Reynolds numbers. Figure 1 shows two typical wind mean speed sequences. The central 96 % of the acceleration and deceleration ramps have a linearity of 1.4 % of the maximum wind speed.

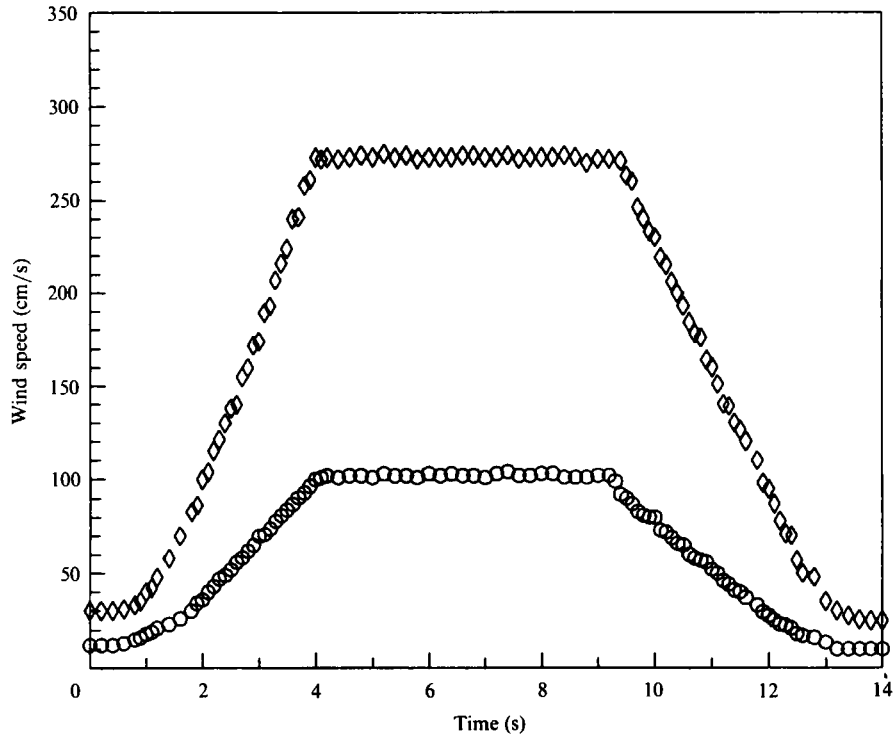

FIGURE 1. Two typical wind tunnel mean speeds as functions of time. Phase average of 20 runs with 200 samples per run.

Five circular cylinders made of 0.64, 1.2, 1.56, 3.2 and 4.8 mm diameter polished drill rod were used in the experiments. The length-to-diameter ratios of these cylinders were between 62 and 468. The large number of cylinders allows for multiple measurements of each dependent variable at identical Reynolds numbers, but with different cylinder diameters. The cylinders were stretched across the wind tunnel by weights. Aeroelastic coupling was prevented by choosing the amount of weight such that the natural frequency of the cylinder was well above vortex street frequencies.

All measurements were made with a constant-temperature hot-wire anemometer using a 4 μm diameter, 1.25 mm working-length tungsten wire. The hot wire was operated at an overheat ratio of 1.8. The hot-wire signal was DC shifted and low-pass filtered at 2 kHz.

Low-speed hot-wire calibrations (0.15–0.9 m/s) were performed in the exit plane of a fully developed laminar pipe flow by a method similar to the one used by Manca, Mastrullo & Mazzei (1988) and Koppius & Trines (1976). The calibration results of the pipe flow method were checked in the wind tunnel by obtaining shedding frequency measurements of the parallel shedding mode. The parallel shedding mode was induced by using a modified version of the end-cylinder technique developed by Eisenlohr & Eckelmann (1989). They used end cylinders with end discs. The end cylinders in the present investigation had a diameter of $2D$ and a length of $11D$, where D is the diameter of the cylinder. They were located at each end of the cylinder, but with a gap of $13D$ between the outer edge of an end cylinder and the wall of the wind tunnel. Figure 2(*a*) shows the spanwise flow visualization of the parallel shedding mode produced by this method. Figure 2(*b*) shows the corresponding oblique shedding mode without end modifications.

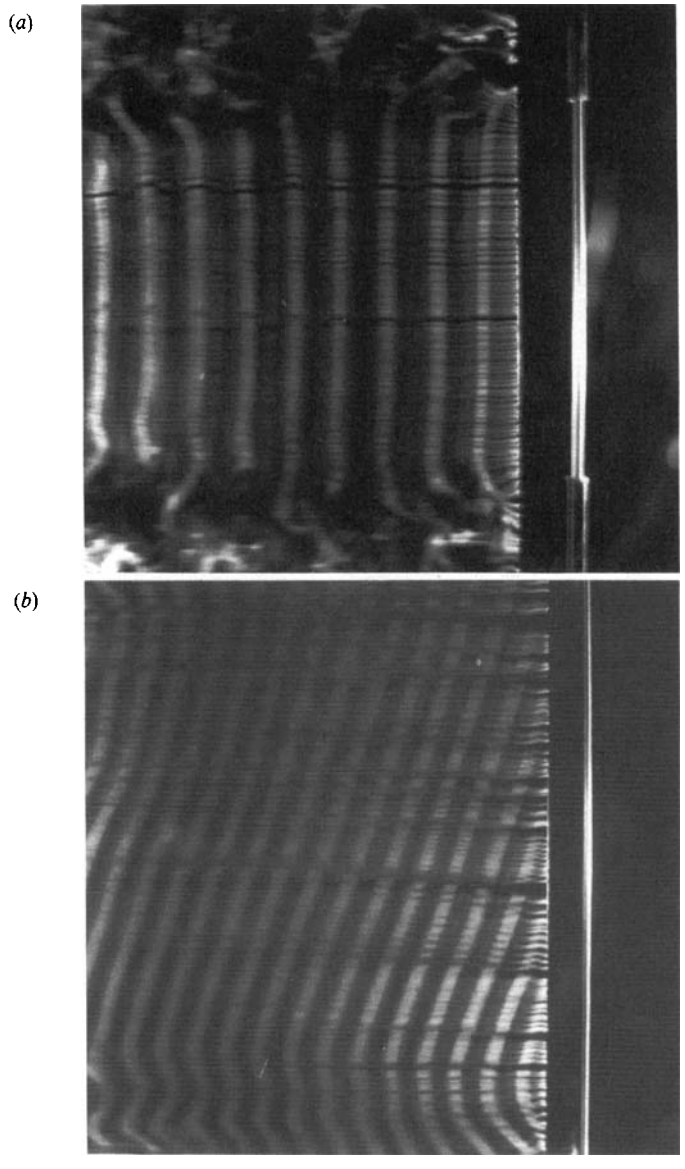

FIGURE. 2. Spanwise flow visualization of the vortex street wake of a circular cylinder, $R = 130$. (*a*) Parallel shedding mode due to end cylinders, (*b*) oblique vortex shedding mode for a cylinder with no end modifications.

Steady flow spectra were obtained from a spectrum analyzer (HP3582A). All other data acquisition and processing were done on an HP200 series computer through an HP6944A multi-programmer. Phase averaging over many cycles was performed whenever mean velocities were measured. This was accomplished by triggering data acquisition in synchronization with the wind tunnel control signal.

3. Results

3.1. *Critical Reynolds number*

Figure 3 shows the signal from a hot wire placed ten diameters downstream ($X/D = 10$) and two diameters out of the centreplane ($Y/D = 2$) of a 1.56 mm diameter cylinder. In this case the flow varies from $R_s = 22$ to $R_f = 195$ with a dimensionless acceleration, $\alpha = 28.5$ ($\alpha = aD^3/\nu^2$, where a is the dimensional acceleration), and then back to $R_s = 22$ with $\alpha = -15.6$. Inset (a) shows the hot-wire signal during the time when periodic fluctuations are first detected. This will be referred to as the onset of the wake instability; apparently these first fluctuations are an indication of the onset of the global temporal instability as defined by Sreenivasan *et al.* (1987) and Provansal *et al.* (1987). Subsequently, the instability disturbs the symmetry of the attached vortices, leading to shedding of the first vortex. The instantaneous critical Reynolds number, R_{ci}, at which the wake instability occurred was 94. Determination of R_{ci} was accomplished by visual inspection of the magnified plots of the hot-wire signal. This method was found to always yield R_{ci} consistent to within ± 0.5. Inset (b) shows the signal while the wake is returning back to symmetric twin attached vortices. The instantaneous Reynolds number at which the periodic wake returned to symmetry was 43.

Figure 4 summarizes the influence of flow acceleration and deceleration on the instantaneous wake critical Reynolds number. Hot-wire measurements to determine the instantaneous critical Reynolds number were typically made at $X/D = 10$ and $Y/D = 2$. However, in order to check the dependence of R_{ci} on X/D some measurements were also made at other X/D. No variation of R_{ci} was found for $5 < X/D < 20$. The cylinder diameters investigated were 0.64, 1.2, 1.56, 3.2 and 4.8 mm. The accompanying Reynolds-number regimes were $25 < R < 175$, $35 < R < 330$, and $22 < R < 195$. The instantaneous Reynolds number at which the onset of wake instability occurred was found to increase with increasing flow acceleration. This demonstrates that the wake is stabilized by flow acceleration. In fact, the mean velocity field in the near wake develops to states that are unstable in steady flow. This is known from measurements showing that the symmetric attached vortices grow to larger lengths than are found in steady flows. For example, in the present investigation the S_e/D ratio attained a value of 3.75 before the near wake became unstable for $\alpha = 98$. The growth of S_e/D with time in an accelerating flow will be further discussed in §3.5.

Figure 4 also shows that the Reynolds number at which the wake returned to symmetry decreased with increasing magnitude of the applied flow deceleration. The critical Reynolds number for zero acceleration was extrapolated to approximately $R_c = 49$. The stabilizing and destabilizing tendencies of the accelerating–decelerating flow on the cylinder wake stability are similar to the established results for internal flows; i.e. acceleration stabilizes a laminar internal flow and deceleration destabilizes the flow (see e.g. Drazin & Reid 1981).

The results shown in figure 4 can be described by two power laws. The equations fitted to the data are

$$R_{ci} = 62.6\alpha^{0.124} \tag{1}$$

for accelerating flows, and

$$R_{ci} = 49.5\,|\alpha|^{-0.0607} \tag{2}$$

for decelerating flows. These results indicate that for a large enough acceleration the wake instability will be suppressed until after the final Reynolds number has been

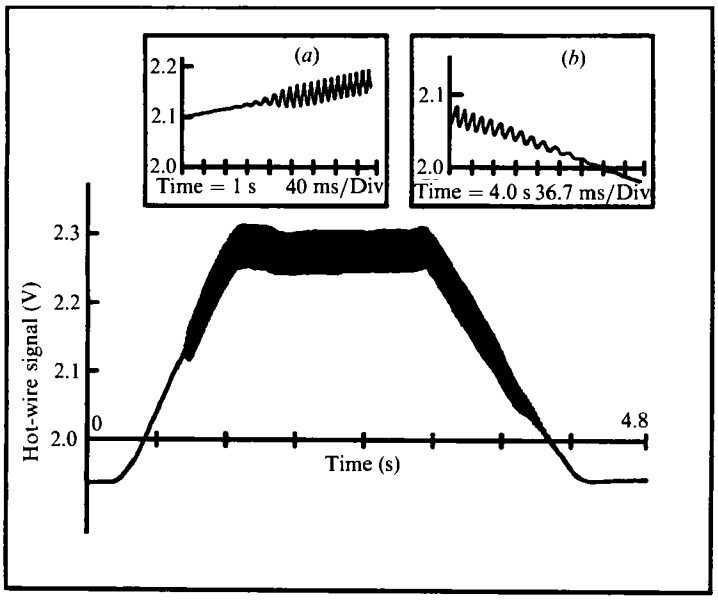

FIGURE 3. Signal from a hot wire located ten diameters downstream and two diameters out of the centreplane of the cylinder. Cylinder diameter is 1.56 mm. Detail (*a*) shows the hot-wire signal during the onset of the wake instability, and detail (*b*) shows the signal while the periodic wake is returning to symmetry.

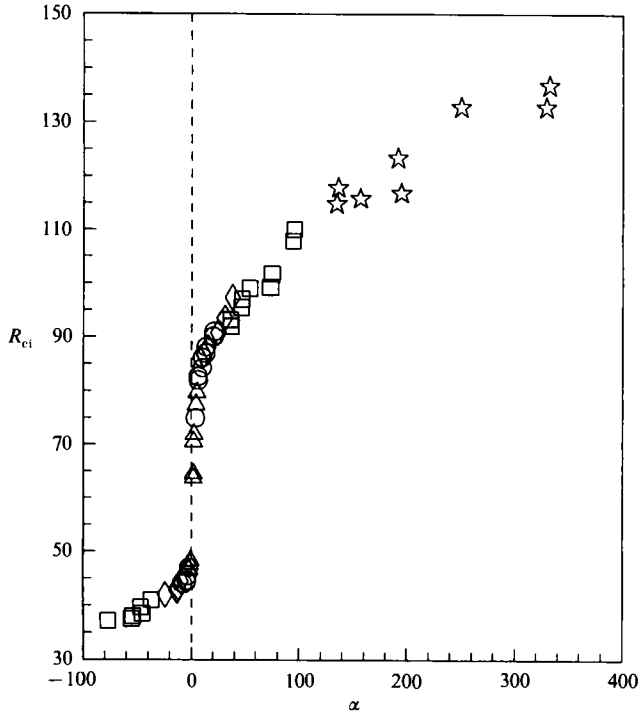

FIGURE 4. Dependence of the instantaneous critical Reynolds number on applied flow acceleration or deceleration. $R_s = 25$; $R_f = 175$: △, $D = 0.64$ mm; ○, $D = 1.2$ mm. $R_s = 22$; $R_f = 195$: ◇, $D = 1.56$ mm. $R_s = 35$; $R_f = 330$: □, $D = 3.2$ mm; ☆, $D = 4.8$ mm.

attained. In other words, disturbances will not amplify at the intermediate supercritical states, provided that the magnitude of the acceleration is large enough, because the transient states are not unstable. For example, equation (1) indicates that at a dimensionless acceleration of 10^4 there will be no growth of the wake instability during the uniform acceleration phase of the flow provided that $R_f \leqslant 195$. In fact, this phenomena has been observed by Sreenivasan *et al.* (1987). They performed rapid, non-uniform acceleration experiments with $R_s = 43$ and $R_f = 49$ and, indeed, the wake oscillations commenced only after the final Reynolds number was attained. The present investigators have conducted similar experiments with a wider span between R_s and R_f and also found that at large enough accelerations the onset of the wake instability occurs after R_f is attained.

3.2 *Critical time*

Figure 5(*a*) shows the dimensionless critical time, τ, elapsed from the start of the acceleration to the onset of the wake instability. This dimensional critical time, t_c, was non-dimensionalized by dividing by the viscous diffusion time, D^2/ν. The cylinders tested were of diameters 0.64, 1.2, 3.2, and 4.8 mm with accompanying Reynolds number ranges of $25 < R < 175$ and $35 < R < 330$. This figure shows that the critical time decreases with increasing flow acceleration. It can be inferred from the results that in the asymptotic case of infinite acceleration (which is equivalent to the case of a flow that is impulsively started from R_s) the wake will become unstable instantaneously. The mechanism leading to this result is that the S_e/D growth rate increases with increasing acceleration (results on S_e/D growth rate are presented in figure 12, below). Thus, the wake attains an unstable configuration very rapidly at large accelerations. In the case of zero acceleration the near wake will ever become unstable, since the Reynolds number always remains below R_c. The best-fit line shown in figure 5(*a*) is the dividing line between two wake flow patterns; (i) wake instability or vortex shedding above the line, and (ii) symmetric attached vortices below the line. The equation of this line is

$$\tau = 75.4\alpha^{-0.914}. \tag{3}$$

Figure 5(*b*) shows the dimensionless critical time, τ, elapsed from the start of deceleration to the wake's return to symmetry. Again, the critical time decreases as the magnitude of the acceleration increases. In the case of zero deceleration the established vortex street will never become stable, since the Reynolds number always remains greater than R_c. In the case of infinite deceleration the wake will become stable instantaneously. The best-fit equation is

$$\tau = 31200(|\alpha|)^{-3.66}. \tag{4}$$

Figure 6(*a*,*b*) shows semi-log plots of the instantaneous critical Reynolds number as function of the dimensionless critical time for accelerating and decelerating flows. The equation for the accelerating flow line was obtained by combining (1) and (3):

$$R_{ci} = 112\tau^{-0.135}. \tag{5}$$

Similarly, for the decelerating flows, combining (2) and (4) yields

$$R_{ci} = 41.6\tau^{0.166}. \tag{6}$$

The curves defined by (5) and (6) represent the dividing lines between the two wake flow patterns.

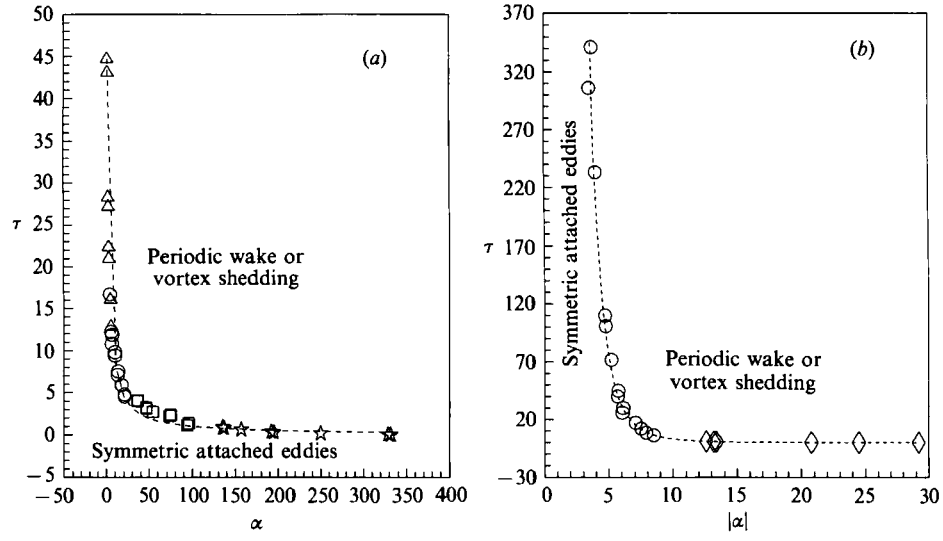

FIGURE 5. Relationship between the dimensionless critical time and the dimensionless applied acceleration and deceleration. (*a*) The time elapsed from the start of the acceleration to the onset of the wake instability, and (*b*) the time elapsed from the start of the deceleration to the wake's return to symmetry. Symbols as in figure 4.

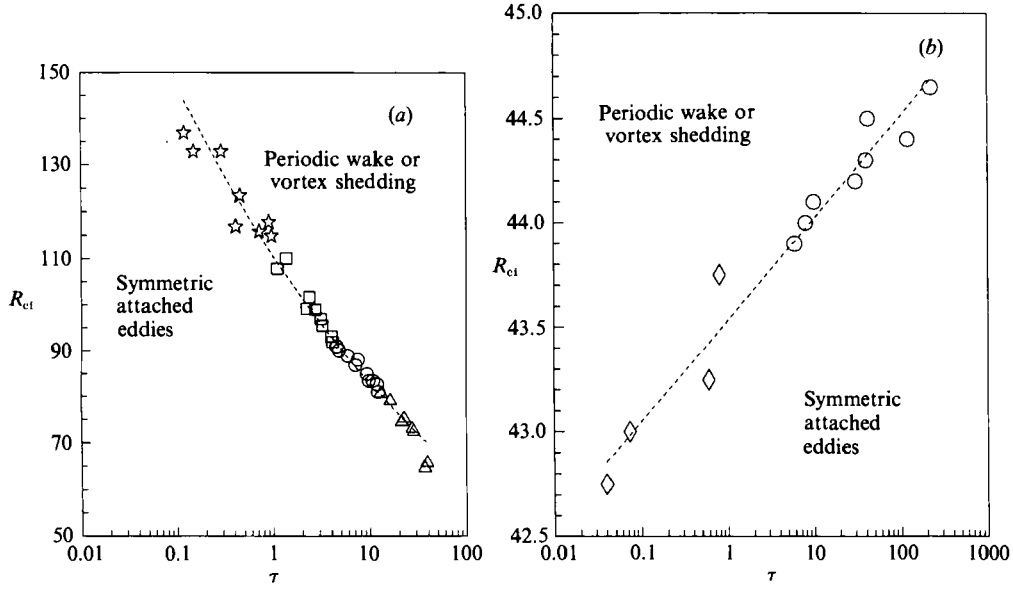

FIGURE 6. Semi-log plots of the instantaneous critical Reynolds number as a function of dimensionless critical time. (*a*) Accelerating flow, and (*b*) decelerating flow. Symbols as in figure 4.

It is also clear from figure 6(*a*) that data from experiments with different initial Reynolds numbers collapse to one curve. This can also be seen in figures 4 and 5(*a*). This suggests that the critical time as well as the critical Reynolds number are both insensitive to the initial Reynolds number (as long as it is below R_c). This result is in agreement with the near-wake development flow visualization results observed by Honji & Taneda (1969), and Taneda (1977). They found that immediately after the

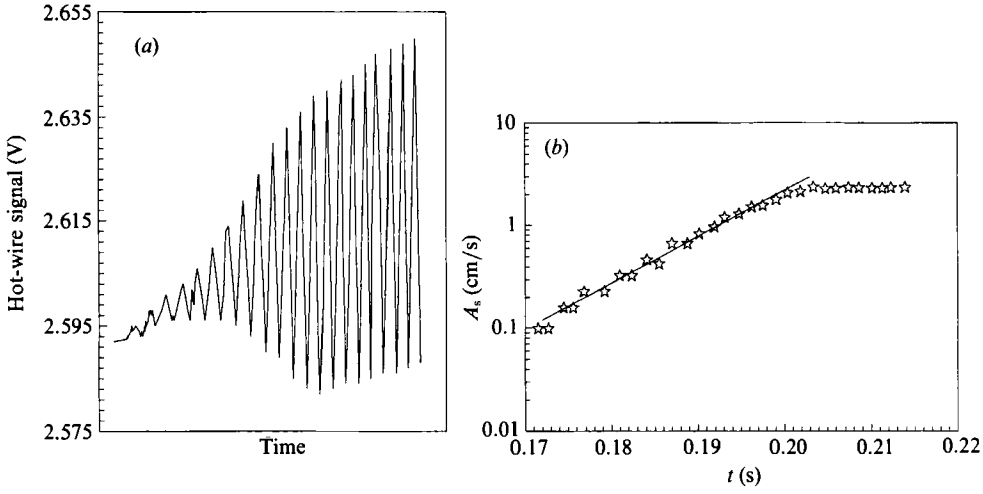

FIGURE 7. Streamwise velocity fluctuations during the onset of the wake instability. (*a*) Magnified view of hot-wire signal, and (*b*) semi-log plot of amplitude envelope. $D = 0.64$ mm, $\alpha = 4.2$, $R_s = 10$, $R_f = 84$, $R_{ci} = 74$.

cylinder was accelerated from $R_s = 20$, the attached vortices were swept downstream and an unseparated flow pattern developed on the cylinder. This was followed by the appearance and growth of new attached vortices. We conclude that the instantaneous critical Reynolds number, the critical time, and the variation of the instantaneous Strouhal number (which will be discussed below) are all a function of acceleration only, i.e. $R_{ci} = R_{ci}(\alpha)$, $\tau = \tau(\alpha)$, and $S_i = S_i(\alpha)$.

The results shown in figures 4, 5(*b*), and 6(*b*) suggest that the critical Reynolds number and critical time in the decelerating flows are insensitive to the Reynolds number at which the flow started to decelerate, R_f. It is not clear what mechanism is responsible for this behaviour.

3.3 *Wake instability growth rate*

The influence of the flow acceleration on the growth of wake instability was also examined. Figure 7(*a*) shows a magnified view of a typical hot-wire signal during the onset of the wake instability. The cylinder diameter was 0.64 mm and the dimensionless acceleration was 4.2. The flow Reynolds number was increased from 10 to 81. It is clear from the figure that in a constant-acceleration flow the amplitude of the wake instability increases exponentially. The maximum amplitude of the disturbance is a function of the final flow Reynolds number and the hot-wire probe location. The exponential growth rate can be described by,

$$A_s = A_1 \exp(\sigma_r(t - t_1)). \tag{7}$$

Here, A_s is the amplitude as a function of time t, σ_r is the growth rate of the disturbance, t_1 is a reference time (any time within the time domain of exponential growth), and A_1 is the amplitude at time t_1.

Figure 7(*b*) shows a semi-log graph of the amplitude of the streamwise velocity fluctuations during the onset of the wake instability. This figure was obtained by rectifying and removing the DC component of the wake signal in figure 7(*a*). The growth rate of the disturbance, σ_r, was 68 s^{-1}, which was determined from the slope of the line shown in figure 7(*b*).

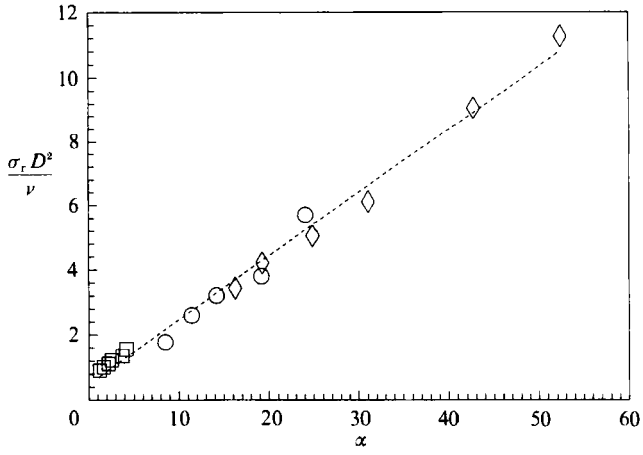

FIGURE 8. Growth rate of the wake instability as a function of the applied flow acceleration. □, $D = 0.64$ mm, $R_s = 10$; $R_f = 81$; ○, $D = 1.2$ mm, $R_s = 12$; $R_f = 97$; ◇, $D = 1.56$ mm, $R_s = 15$; $R_f = 108$.

Figure 8 shows the growth rate of the disturbance as a function of the dimensionless flow acceleration. The hot-wire probe was located at $X/D = 10$ in all cases. The Y/D values corresponding to the cylinder diameter were 1.5 for $D = 0.64$ mm, 1 for $D = 1.2$ mm, and 2 for $D = 1.56$ mm. The Reynolds-number ranges investigated were 10 to 81, 12 to 97, and 15 to 108. The growth rate was non-dimensionalized by the diffusion timescale, ν/D^2. The best-fit equation to the data is

$$\sigma_r D^2/\nu = 0.197\alpha + 0.39. \tag{8}$$

The slope of the growth rate as a function of acceleration, $\mathrm{d}(\sigma_r D^2/\nu)/\mathrm{d}\alpha = 0.197$, is constant and is independent of α, R_s and R_f for the range of these parameters that was investigated. The present results are for the streamwise velocity component. However, it is thought that the growth rate of the transverse velocity fluctuations will be the same as that of the streamwise fluctuations; this is supported by the results of the impulsively started flow experiments of Sreenivasan *et al.* (1987) employing single-hot-wire anemometry and that of Provansal *et al.*'s (1987) measurements using two-component LDV. By impulsively starting a circular cylinder from a subcritical Reynolds number to a supercritical Reynolds number, these investigators observed that the growth of the disturbance with Reynolds number, $\mathrm{d}(\sigma_r D^2/\nu)/\mathrm{d}R$, was a constant value of 0.2. However, the starting and the final Reynolds numbers were kept near to R_c in their experiments, and the wake instability was not allowed to grow in the intermediate supercritical Reynolds-number range as in the present case.

3.4. *Limit-cycle shedding frequency*

The influence of flow acceleration on limit-cycle shedding frequency was also investigated. Figure 9(*a*) shows the variation of the instantaneous Strouhal number, $S_i = fD/U$ (f is the limit-cycle velocity fluctuation frequency calculated from the hot-wire signals) with instantaneous Reynolds number, R_i, at four accelerations. Cylinders of 1.2 and 1.56 mm diameters were used with accompanying Reynolds-number ranges of $25 < R < 175$ and $22 < R < 195$. The results reveal that the instantaneous Strouhal number decreased with increasing applied acceleration. This

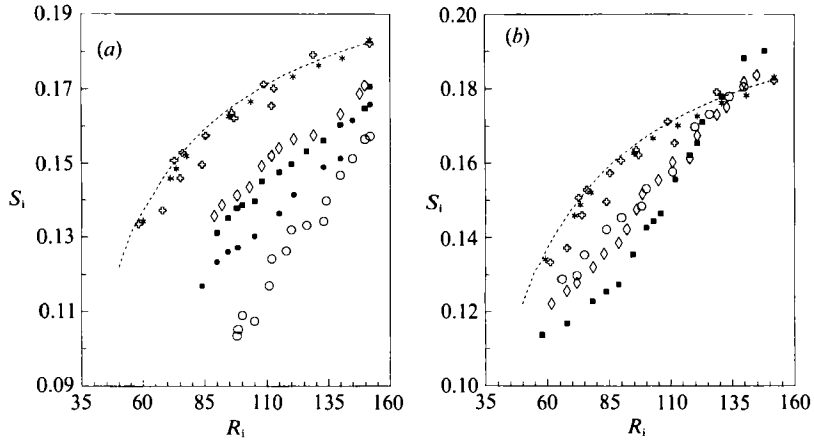

FIGURE 9. The dependence of the instantaneous Strouhal number on applied flow acceleration and deceleration. (*a*) Accelerating flow. $R_s = 25$, $R_f = 175$, and $D = 1.2$ mm: ●, $\alpha = 16.2$; ○, $\alpha = 18.5$. $R_s = 22$, $R_f = 195$; $D = 1.56$ mm: ◇, $\alpha = 10.8$; ■, $\alpha = 12.4$. (*b*) Decelerating flow. $R_s = 25$, $R_f = 175$; $D = 1.2$ mm: ○, $\alpha = -11.5$. $R_s = 22$, $R_f = 195$; $D = 1.56$ mm: ◇, $\alpha = -9.8$; ■, $\alpha = -3.6$. Steady flow results ($\alpha = 0$) are shown in both (*a*) and (*b*): ------, Roshko (1954*a*) *S*–*R* curve; present measurements ⌖, $D = 1.2$ mm; *, $D = 1.56$.

figure also shows the present steady flow data (with end modifications) along with the empirical *S*–*R* relationship from Roshko (1954*a*). All accelerating flow results are below the Roshko curve. It can be inferred from the results that the Strouhal number at a given Reynolds number will approach zero for very large acceleration. The observed reduction is due to the lag in shedding frequency as the flow accelerates. Gerrard (1966) notes that reduction in shedding frequency is linked to elongation of the formation region of the wake. Apparently, in the present case, the accelerating flow causes a rapid build-up of vorticity behind the cylinder with little time for cross-wake vorticity transfer. Thus, the formation region is elongated and the shedding frequency reduced. The reduction in Strouhal number is also observed for the steady flow over small-aspect-ratio cylinders ($L/D < 40$, Nishioka & Sato 1974; Gerich & Eckelmann 1982; Gerich 1986; Williamson 1989; Lee & Budwig 1990) as well as in steady flow over cylinders that have a splitter plate attached on the downstream side (Roshko 1954*b*).

Figure 9(*a*) also suggests that the S_i–R_i curves are continuous for accelerating flows. The absence of the first discontinuity in the S_i–R_i curve implies that the oblique shedding which originates from the cylinder end and the wall of the wind tunnel does not have time to propagate in an accelerating flow. It, therefore, leaves the midspan of the wake flow uncontaminated and results in a continuous S_i–R_i curve.

The variation of the instantaneous Strouhal number with deceleration is shown in figure 9(*b*). The results indicate that the instantaneous Strouhal number increases with increasing magnitude of deceleration. This trend makes sense in the light of the above formation-length model. However, it is not clear why all the Strouhal number results measured during deceleration are below Roshko's *S*–*R* relationship. Furthermore, the Strouhal number for zero deceleration cannot be extrapolated from the present results.

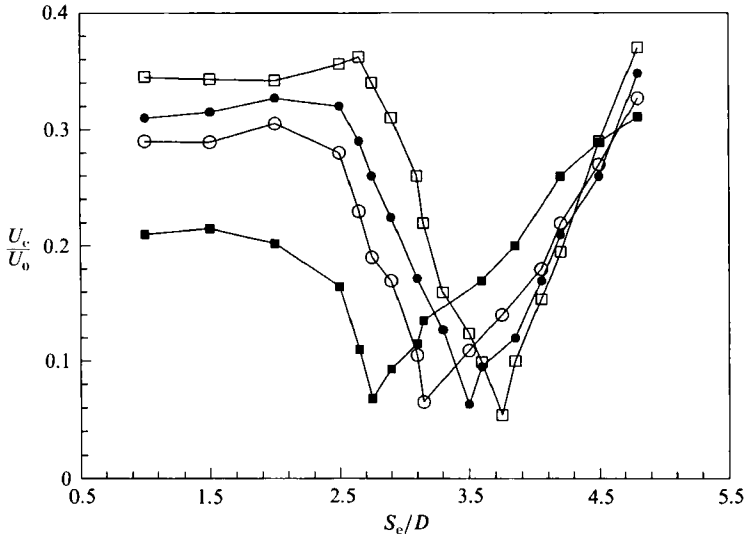

FIGURE 10. Instantaneous velocity measurements in the centreplane behind a circular cylinder. Each curve shows the variation of velocity with distance from the cylinder at a particular dimensionless time, τ. The cusp in each velocity curve indicates the location of the rear wake stagnation point at that time. $\alpha = 98$, $R_s = 20$; $R_f = 185$; □, $\tau = 1.11$; $R_i = 105$; ●, $\tau = 1.02$; $R_i = 97$; ○, $\tau = 0.93$; $R_i = 88$; ■, $\tau = 0.77$; $R_i = 73$.

3.5 *Closed wake length and growth rate*

Instantaneous values of the closed wake length, S_e, were obtained from hot-wire measurements in the centreplane of the cylinder wake. Figure 10 shows a typical instantaneous velocity development as a function of downstream distance in an accelerating flow. The time variation of the mean velocity along the wake centreplane was obtained from phase-averaged hot-wire measurements of 60 runs with 200 samples per run. The cusp in each velocity profile indicates the location of the rear wake stagnation point. An ultimate vortex-eddy length of 3.75 cylinder diameters was determined at $\tau = 1.11$. The time-development of the closed wake length shown in figure 10 verifies that, (i) the wake vortices are stabilized by the acceleration of the oncoming flow, and (ii) S_e/D grows larger than 2.2, which is the accepted value for steady flow over a circular cylinder.

The use of a hot wire in the recirculating wake region of a cylinder has been the subject of some concern since the hot wire may disturb the wake. On the one hand there is evidence that meaningful results on closed wake length can be obtained from hot-wire data. Figure 3 in Nishioka & Sato (1978) shows a comparison of steady-flow wake length results made by several investigators. The hot-wire results obtained by Nishioka are in good agreement with the flow visualization and numerical results that are also shown. On the other hand, there are the results reported in Strykowski & Sreenivasan (1990) that demonstrate how a control cylinder in the vicinity of the near wake can cause significant changes in the stability of the wake. However, these experiments were done with a relatively large diameter 'control cylinder' which extended the entire length of the main cylinder, while in the present experiments the hot wire is a very small diameter cylinder extended over about 1% of the length of the cylinder. The results presented below show reasonable trends that do not appear to be influenced by disturbances from the hot wire.

Figure 11 (*a*) shows results on the time evolution of S_e/D at four different flow

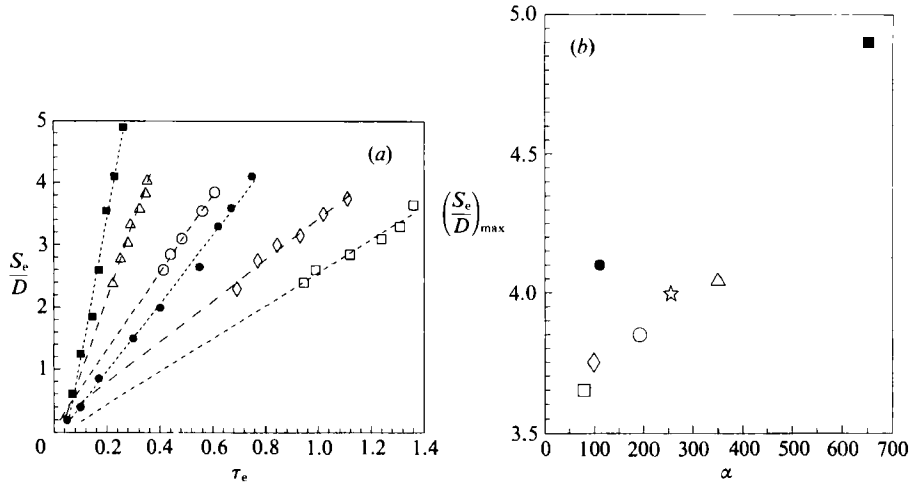

FIGURE 11. (*a*) Growth of closed wake length as a function of the time at different accelerations. The maximum S_e/D at a given acceleration is shown by the uppermost data point on each line. (*b*) Maximum closed wake length as a function of acceleration. Present measurements: □, $\alpha = 79$, $R_s = 18$; $R_f = 135$; ◇, $\alpha = 98$, $R_s = 20$; $R_f = 185$; ○, $\alpha = 192$, $R_s = 22$; $R_f = 235$; ☆, $\alpha = 255$, $R_s = 25$; $R_f = 260$; △, $\alpha = 350$, $R_s = 28$; $R_f = 280$. Honji & Taneda's (1969) measurements with $R_s = 20$ and $R_f = 110$: ●, $\alpha = 110$ and ■, $\alpha = 652$.

accelerations. These were obtained by the above method (figure 10). The top data point on each line in the figure is the last data point that could be measured before the onset of the wake instability. These points represent the maximum S_e/D that can be attained at a given acceleration. Figure 11(*b*) shows the maximum S_e/D as a function of acceleration. The results of figure 11(*a*,*b*) reveals that, (i) the maximum S_e/D increases with flow acceleration, and (ii) the time growth rate of S_e/D increases with applied flow acceleration. As previously pointed out, these results verify the hypothesis that the wake is stabilized by an applied flow acceleration. Figure 11(*a*,*b*) also shows results from Honji & Taneda (1969). They found a greater maximum S_e/D than in the present experiments; however, the L/D ratios used in their experiments were between 4 and 20. It is clear that the confining walls influence the stability of the wake, even in an accelerating flow. The combined effects of applied flow acceleration and confining walls are further discussed in §3.6.

The results shown in figure 11(*b*) also indicate that the maximum S_e/D values appear to approach a limiting value at large accelerations. The values lie below S_e/D of 4.3, which was observed by Taneda (1977) for an impulsively started cylinder flow.

The physical explanation of the elongation of the S_e/D ratio in an accelerating flow can be understood as follows. In the early stages of motion vorticity does not have time to diffuse and so accumulates rapidly in the closed wake vicinity of the cylinder. The growth of the vortices is so rapid that the vortices become much larger than the corresponding steady case before they separate from the shear layer. It is, therefore, apparent that the wake development (which is a function of R_i and α) will lag behind what is observed in a steady flow at the same Reynolds number. The increase of the maximum of S_e/D with increasing acceleration in figure 11(*b*) can also be explained based on the above hypothesis. That is, the larger the acceleration, the more rapid the vorticity accumulation. This tendency indicates less vorticity transfer across the wake centreline, and leads to a large final value of S_e/D and a more stabilized wake.

Figure 12 shows that the time growth rate of S_e/D is a linear function of the

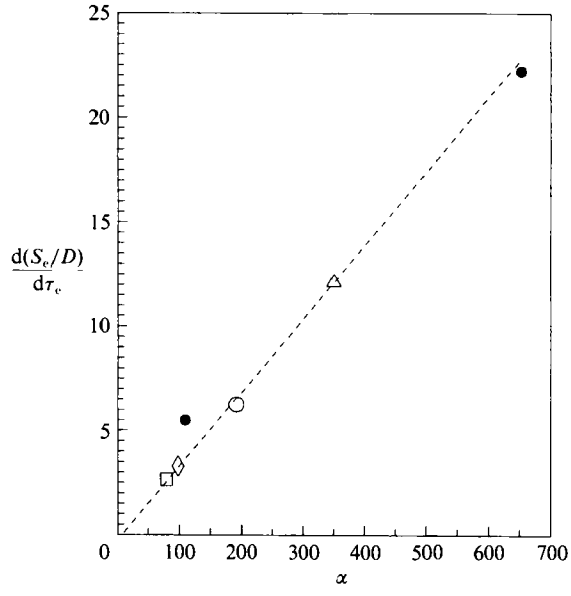

FIGURE 12. Time growth rate of the closed wake length ratio as a function of the dimensionless acceleration. Symbols as in figure 11.

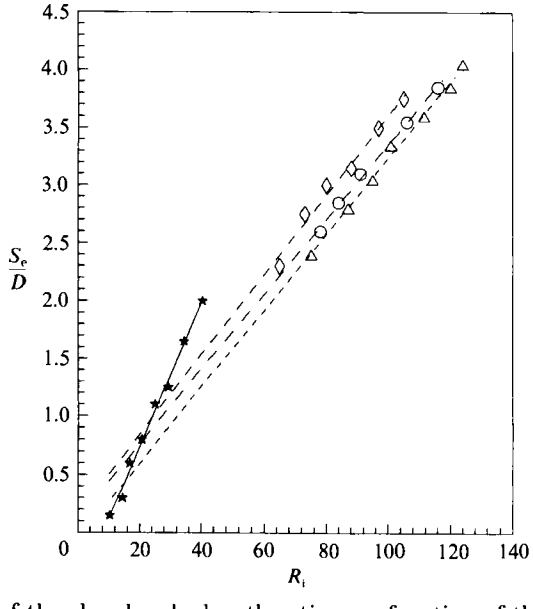

FIGURE 13. Growth of the closed wake length ratio as a function of the instantaneous Reynolds number at four accelerations. Present measurements: symbols as in figure 11. Coutanceau & Bouard (1977*a*): ★, $\alpha = 0$.

applied flow acceleration. Honji & Taneda's (1969) measurements are also shown in this figure by solid circles. The equation fitted to the data is

$$d(S_e D)/d\tau = 0.0344\alpha + 0.016. \tag{9}$$

Figure 13 shows the linear relationship between S_e/D and R_i at three different flow accelerations. The results show that the growth of the closed wake can be stabilized

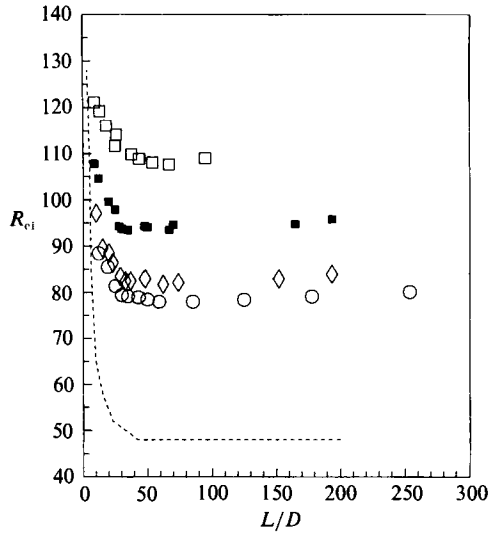

FIGURE 14. Combined stabilizing effects of the flow acceleration and the end plates. Present measurements with $D = 3.2$ mm, $R_s = 33$, $R_f = 365$: □, $\alpha = 150$. $D = 1.56$ mm, $R_s = 28$, $R_f = 186$: ■, $\alpha = 34.1$; ◇, $\alpha = 13.3$. $D = 1.2$ mm, $R_s = 23$, $R_f = 167$: ○, $\alpha = 7$. Nishioka & Sato (1974): ------, $\alpha = 0$.

to a higher R_1 with a larger α. Steady flow measurements from Coutanceau & Bouard (1977*a*) are also shown in this figure (solid stars). The slope of the S_e/D lines, $\mathrm{d}(S_e/D)/\mathrm{d}R_1$, was found to be the constant value of 0.033 at all three flow accelerations. This is about one-half of the slope for a steady flow (determined from Coutanceau & Bouard's data).

3.6 *Effect of cylinder length-to-diameter ratio*

Figure 14 shows the combined effects of cylinder length-to-diameter ratio and applied flow acceleration on the onset of the wake instability. For these experiments end plates similar to the Nishioka & Sato (1974) design were fitted to the test cylinders so that the cylinder aspect ratio could be varied. The results show that the confining wall effects begin to appear for cylinder aspect ratio smaller than about 25, when the flow is accelerating. Similar stabilizing results are also observed for steady flows by Shair *et al.* (1963), Nishioka & Sato (1974), Mathis, Provansal & Boyer (1984), Sreenivasan *et al.* (1987), and Lee & Budwig (1990). However, these investigators found that the wake was stabilized for L/D smaller than about 40. Nishioka & Sato's results for steady flow are shown on the figure as a dashed line.

4. Summary and conclusions

We have presented results to describe the influence of flow acceleration on the time evolution of a cylinder wake just before, during, and immediately after the onset of the wake instability. The results are summarized by the following conclusions.

(i) The wake is stabilized by flow acceleration; therefore the onset of the wake instability occurs at larger Reynolds numbers than in the steady flow case and the mean velocity field in the near wake develops to states that would be unstable in a steady flow. In the case of flow deceleration, the wake is destabilized.

(ii) The temporal growth rate of the wake instability is directly proportional to the applied flow acceleration.

(iii) The time from the start of acceleration to the onset of the wake instability (the critical time) decreases with increasing flow acceleration. The mechanism behind this result is that S_e/D growth rates increase with increasing acceleration. Thus, the wake attains an unstable configuration very rapidly at large accelerations. For decelerating flows, the time from the start of deceleration to the wake's return to symmetry also decreases with increasing magnitude of deceleration.

(iv) The instantaneous Strouhal number decreases with increasing applied acceleration. All accelerating flow S–R results are continuous and below steady flow results. The observed reduction in Strouhal number is well accounted for by the mechanism of applied acceleration leading to elongation of the wake formation region.

(v) For constant applied acceleration, the instantaneous critical Reynolds number, the critical time, and the instantaneous Strouhal number are all independent of the initial Reynolds number as well as the final Reynolds number, provided that the initial Reynolds number is less than R_c.

(vi) The closed wake length is directly proportional to the applied flow acceleration, and the maximum S_e/D ratio is exponentially related to the flow acceleration.

(vii) The time growth rate of S_e/D increases linearly with dimensionless acceleration.

(viii) The slope of the S_e/D ratio lines, $\mathrm{d}(S_e/D)/\mathrm{d}R_i$, was found to have a constant value of 0.033 for the accelerating flows, which is about one-half of the slope for a steady flow.

(x) The confining wall effects appear for cylinder aspect ratio smaller than about 25, when the flow is accelerated.

The present experiments have concentrated on unsteady flows with initial Reynolds number lower than the steady flow critical Reynolds number. Future experiments should consider the influence of applied unsteadiness on an established vortex street ($R_i > R_c$). It is also thought that full field measurements of the near-wake development are required in order to achieve a better understanding of the wake instability as well as the initial stages of vortex shedding.

REFERENCES

Berger, E. & Wille, R. 1972 Periodic flow phenomena. *Ann. Rev. Fluid Mech.* **4**, 313–340.

Bouard, R. & Coutanceau, M. 1980 The early stage of development of the wake behind an impulsively started cylinder for $40 < Re < 10^4$. *J. Fluid Mech.* **101**, 583–607.

Coutanceau, M. & Bouard, R. 1977*a* Experimental determination of the main features of the viscous flow in the wake of a circular cylinder in uniform transition. Part 1. Steady flow. *J. Fluid Mech.* **79**, 231–256.

Coutanceau, M. & Bouard, R. 1977*b* Experimental determination of the main features of the viscous flow in the wake of a circular cylinder in uniform transition. Part 2. Unsteady flow. *J. Fluid Mech.* **79**, 257–272.

Drazin, P. G. & Reid, W. H. 1981 *Hydrodynamic Stability*. Cambridge University Press.

Eisenlohr, H. & Eckelmann, H. 1989 Vortex splitting and its consequences in the vortex street wake of cylinder at low Reynolds number. *Phys. Fluids* A **1**, 189–192.

Friehe, C. A. 1980 Vortex shedding from cylinder at low Reynolds numbers. *J. Fluid Mech.* **100**, 237–241.

Gerich, D. 1986 A limiting process for the von Kármán street showing the change from two- to three-dimensional flow. In *Flow Visualization*, vol. 4 (ed. C. Véret), pp. 463–467. Hemisphere.

Gerich, D. & Eckelmann, H. 1982 Influence of end plates and free ends on the shedding frequency of circular cylinders. *J. Fluid Mech.* **122**, 109–121.

GERRARD, J. H. 1966 The mechanics of the formation region of vortices behind bluff bodies. *J. Fluid Mech.* **25**, 401–413.

HONJI, H. & TANEDA, S. 1969 Time-dependent flow around a circular cylinder accelerated uniformly from one steady speed to another. *Rep. Res. Inst. for Appl. Mech.*, vol. XVII, no. 9, pp. 187–193.

KARNIADAKIS, G. E. & TRIANTAFYLLOU, G. S. 1989 Frequency solution and asymptotic states in laminar wake. *J. Fluid Mech.* **199**, 441–469.

KOPPIUS, A. M. & TRINES, G. R. M. 1976 The dependence of hot wire probes calibration on gas temperature at low Reynolds numbers. *Intl. J. Heat Mass Transfer* **19**, 967–974.

LEE, T. & BUDWIG, R. 1991 A study of the effect of aspect ratio on vortex shedding behind circular cylinders. *Phys. Fluids* A **3**, 309–315.

MANCA, O., MASTRULLO, R. & MAZZEI, P. 1988 Calibration of hot wire probes at low velocities in air with variable temperature. *Dantec Information No.* 06, pp. 6–8.

MATHIS, C., PROVANSAL, M. & BOYER, L. 1984 The Bénard–von Kármán instability: An experimental study near the threshold. *J. Physique Lett.* **45**, L-483–L-491.

MONKEWITZ, P. A. 1988 The absolute and convective nature of instability in two-dimensional wakes at low Reynolds numbers. *Phys. Fluids* **31**, 999–1006.

NISHIOKA, M. & SATO, H. 1974 Measurements of velocity distributions in the wake of a circular cylinder at low Reynolds numbers. *J. Fluid Mech.* **65**, 97–112.

NISHIOKA, M. & SATO, H. 1978 Mechanism of determination of the shedding frequency of vortices behind a cylinder at low Reynolds numbers. *J. Fluid Mech.* **89**, 49–60.

PROVANSAL, M., MATHIS, C. & BOYER, L. 1987 Bernard–von Kármán instability: Transient and forced regimes. *J. Fluid Mech.* **182**, 1–22.

ROSHKO, A. 1954*a* On the development of turbulent wakes from vortex streets. *NACA Rep.* 1191, pp. 801–825.

ROSHKO, A. 1954*b* On the drag and shedding frequency of two-dimensional bluff bodies. *NACA Tech. Note* 3169, p. 29.

SARPKAYA, T. 1963 Lift, drag, and added-mass coefficients for a circular cylinder immersed in a time-dependent flow. *Trans. ASME : J. Appl. Mech.* **30**, 13–15.

SARPKAYA, T. 1978 Impulsive flow about a circular cylinder. *Naval Postgraduate School Tech. Rep.* NPS-69SL-78-008.

SHAIR, F. H., GROVE, A. S., PETERSON, E. E. & ACRIVOS, A. 1963 The effect of confining walls on the stability of steady wake behind a circular cylinder. *J. Fluid Mech.* **17**, 546–550.

SREENIVASAN, K. R., STRYKOWSKI, P. J. & OLINGER, D. J. 1987 Hopf bifurcation, Landau equation, and vortex shedding behind circular cylinders. In *Forum on Unsteady Flow Separation*, FED-Vol 52, pp. 1–13. ASME.

STRYKOWSKI, P. J. & SREENIVASAN, K. R. 1990 On the formation and suppression of vortex 'shedding' at low Reynolds numbers. *J. Fluid Mech.* **218**, 71–107.

TANEDA, S. 1977 Visual study of unsteady separation flows around bodies. *Prog. Aerospace Sci.* **17**, 287–348.

TRITTON, D. J. 1959 Experiments of the flow past a circular cylinder at low Reynolds numbers. *J. Fluid Mech.* **6**, 547–567.

TRITTON, D. J. 1971 A note on the vortex streets behind circular cylinder. *J. Fluid Mech.* **45**, 203–208.

WILLIAMSON, C. H. K. 1989 Oblique and parallel modes of vortex shedding in the wake of a circular cylinder at low Reynolds numbers. *J. Fluid Mech.* **206**, 579–627.